ARTICLE IN PRESS

Available online at www.sciencedirect.com
ScienceDirect

Pattern Recognition ▮▮▮ (▮▮▮▮) ▮▮▮–▮▮▮

PATTERN RECOGNITION
THE JOURNAL OF THE PATTERN RECOGNITION SOCIETY

www.elsevier.com/locate/pr

Optic disk feature extraction via modified deformable model technique for glaucoma analysis

Juan Xu[a,*], Opas Chutatape[b], Eric Sung[c], Ce Zheng[d], Paul Chew Tec Kuan[d]

[a]*Department of Ophthalmology, School of Medicine, University of Pittsburgh, USA*
[b]*Department of Electrical and Computer Engineering, Rangsit University, Thailand*
[c]*School of Electrical and Electronic Engineering, Nanyang Technological University, Singapore*
[d]*Ophthalmology Department, National University Hospital, Singapore*

Received 25 September 2005; received in revised form 15 June 2006; accepted 5 October 2006

Abstract

A deformable-model based approach is presented in this paper for robust detection of optic disk and cup boundaries. Earlier work on disk boundary detection up to now could not effectively solve the problem of vessel occlusion. The method proposed here improves and extends the original snake, which is essentially a deforming-only technique, in two aspects: knowledge-based clustering and smoothing update. The contour deforms to the location with minimum energy, and then self-clusters into two groups, i.e., edge-point group and uncertain-point group, which are finally updated by the combination of both local and global information. The modifications enable the proposed algorithm to become more accurate and robust to blood vessel occlusions, noises, ill-defined edges and fuzzy contour shapes. The comparative results on the 100 testing images show that the proposed method achieves better success rate (94%) when compared to those obtained by GVF-snake (12%) and modified ASM (82%). The proposed method is extended to detect the cup boundary and then extract the disk parameters for clinical application, which is a relatively new task in fundus image processing. The resulted cup-to-disk (C/D) ratio shows good consistency and compatibility when compared with the results from Heidelberg Retina Tomograph (HRT) under clinical validation.

Keywords: Boundary detection; Optic disk; Cup; Snake; Deformable model; Fundus image

1. Introduction

Optic disk with bright-white region inside called pallor is one of main components on the fundus image as shown in Fig. 1(a). It is the entrance of the optic nerve and blood vessels to the retina. The 3-D shape of the optic disk is an important indicator of various ophthalmic pathologies. For an instance, the optic disk becomes bigger and deeper in the eyes with glaucoma. Clinicians quantify the cupping of the optic disk to evaluate the progression of glaucoma, where cup is defined at certain depth down from the disk edges. Cup and disk boundaries act as the references to quantitative measurements of the disk parameters, such as cup-to-disk (C/D) vertical ratio, C/D area ratio, etc., which are the important parameters for diagnosis. The existing ophthalmic instrument used to analyze the optic disk such as Optical Coherence Tomography (OCT) and Heidelberg Retina Tomograph (HRT) are based on scanning laser technique that can provide a colorless or pseudo-color 3-D visualization. The clinicians must manually place the disk boundary on the 3-D image as the reference, and then the cup boundary can be generated from the disk contour based on 3-D depth information. Since the image created from OCT or HRT is not true color image, the 2-D color fundus image is still referred to by most clinicians for the estimation of disk and cup boundaries. As an effective solution to this, a fully automated approach of cup and disk boundary detection is

* Corresponding author. Ophthalmology and Visual Sciences Research Center, University of Pittsburgh, Eye and Ear Institute, 203 Lothrop Street, Suite 827, Pittsburgh, PA 15213, USA. Tel.: +1 412 647 0372; fax: +1 412 647 5119.
E-mail address: xxujuan@pmail.ntu.edu.sg (J. Xu).

0031-3203/$30.00
doi:10.1016/j.patcog.2006.10.015

Please cite this article as: J. Xu, et al., Optic disk feature extraction via modified deformable model technique for glaucoma analysis, Pattern Recognition (2006), doi: 10.1016/j.patcog.2006.10.015

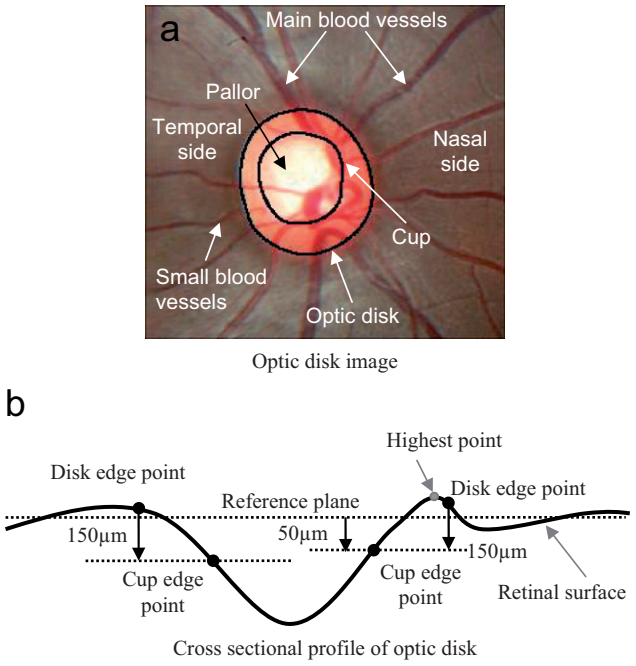

Fig. 1. Definition of cup and disk contours: (a) optic disk image; (b) cross sectional profile of optic disk.

presented in this paper to provide essential disk parameters for clinical analysis and pathological monitoring.

The optic disk generally appears as a bright circular or elliptic region. The methods of optic disk boundary detection can be separated into two steps: optic disk localization and disk boundary detection. Correct localization of the optic disk may improve the accuracy of disk boundary extraction. Many existing approaches can be used to locate the optic disk with reasonable success. Sinthanayothin [1] located the position of the optic disk by finding the region with the highest local variation in the intensity. Tamur [2] and Pinz [3] applied Hough transform to obtain optic disk center and the outer circle of disk boundary. Recently, a principal component analysis (PCA) model based approach was used in Ref. [4], and template matching was used in Refs. [5–7]. Hoover [8] utilized the geometric relationship between the optic disk and main blood vessels to identify the disk location, similar approaches were introduced in Refs. [9,10]. Correctly locating the optic disk is the first and essential step for optic disk segmentation. Subsequently the disk center is estimated and used to initialize the disk boundary.

Interference of blood vessels is one of the main difficulties to segment the optic disk reliably and accurately. This problem is very similar to other boundary detection and image segmentation problems in medical imaging area that still require robust solution. Currently, deformable models offer a reasonable approach for boundary detection and image segmentation which can be roughly classified into two categories: free-form deformable models, such as snakes, and parametrically deformable models, such as active shape models (ASMs). Mendels et al. [11] and Osareh et al. [6] extracted the optic disk boundary by GVF-snake algorithm, in which the blood vessel was first removed by morphology in the preprocessing step. Walter et al. [12] also used morphological filtering techniques to remove the blood vessels and then detected the optic disk boundary by means of shade-correlation operation and watershed transformation. Although the morphology preprocessing helps reduce the effect of blood vessels, it could not totally remove the effect. The resulted boundary was distorted in the regions with outgoing vessels. Li and Chutatape [13,14] used a PCA method to locate the optic disk and an ASM to refine the disk boundary. Although this approach could indirectly handle blood vessel occlusion problem with moderate accuracy, by using shape models, the fuzzy shapes of optic disk due to various pathological changes were not easy to be represented by a number of shape models, which might reduce the accuracy of the result. Parametrically deformable models (ASM method) are suitable for use when more specific shape information is available and the detected object has relatively uniform shape with limited variation. However, in optic disk boundary detection, pathological changes may arbitrarily deform the shape of optic disk and also distort the course of blood vessels. Hence, deformable templates may not be able to sufficiently encode various shapes of optic disk from different pathological changes. Lowell et al. [7] segmented the optic disk by a contour deformation method based on a global elliptic model and a local deformable model with variable edge-strength dependent stiffness. However, the authors indicated that the performance to the images with variably pathological changes still needed to be further improved. A level set approach was introduced in Ref. [15], which can segment the objects with arbitrarily complex shapes. The advantage of this approach is its ability to evolve the model in the presence of sharp corners, cusps, shapes with pieces and holes, etc. Nevertheless, many of these problems are different from those encountered in the boundary detection of optic disk. How to remove the influence of blood vessels is still the main difficulty to the employment of the above-mentioned methods to the optic disk boundary detection.

Cup is the depressed area inside the optic disk, hence the 3-D depth is the primary feature of the cup boundary, for which the automated detection is a relatively new task and challenging work in fundus image processing. So far, very few researchers focused their work on cup boundary detection due to the fact that the 3-D image is not easily available. Results of disk and cup boundaries were shown in Ref. [16], however, the authors did not clearly describe how to obtain these boundaries.

Since 3-D images are not generally available, some definitions are provided to estimate the cup boundary on 2-D images. Previously, the clinicians used the pallor to estimate the cup boundary, while pallor is defined as the area of maximum color contrast inside the disk area. However, in many cases, there is no obvious pallor in the disk area.

Please cite this article as: J. Xu, et al., Optic disk feature extraction via modified deformable model technique for glaucoma analysis, Pattern Recognition (2006), doi: 10.1016/j.patcog.2006.10.015

Even if the pallor is clear, its edge is just close to, but not the exact cup edge. Currently, the bending of small blood vessels at the cup edge is used as a clue to measure the cup boundary. Nevertheless, this method can only provide several points of cup boundary in the area where there are small blood vessels; for the area without small blood vessels, the cup boundary is not easy to be estimated. Alternatively, 3-D depth information is a relatively reliable feature to estimate the cup contour. There are several different cup definitions based on depths. In Ref. [17], cup is defined to be 50 μm down from a reference plane which is estimated from the periphery of retinal surface, Another definition [18–22] locates cup at 150, 120 μm, 50%, $\frac{1}{3}$, etc., drop from the optic disk edge to the deepest point as shown in Fig. 1(b). All these cup definitions only depend on the depth information, because the 3-D image obtained in most of these literatures is colorless or only with pseudo-color.

In this paper, a novel approach for automated detection of cup and disk boundaries is proposed based on free-form deformable model technique (snake). The boundaries are extracted based on the combined information of smoothness, gradient, depth, etc. The algorithm extends the original snake technique further in two aspects to directly solve the problem of the influence of blood vessels without affecting the accuracy.

2. Optic disk boundary detection

The original deforming-only snake process is modified and implemented with further two extensions. Firstly, after each deformation, the contour points are classified into edge-point cluster or uncertain-point cluster by knowledge-based unsupervised learning. Secondly, the contour is updated through variable sample numbers. The updating is self-adjusted using both global and local information so that the balance on contour stability and accuracy can be achieved. The proposed method of optic disk boundary detection includes initialization of optic disk boundary, contour deformation, clustering, and smoothing update, which is depicted in a closed-loop block diagram as shown in Fig. 2.

2.1. Energy definition and contour deformation

According to Kass et al. [23], the snake is defined as a parametric curve $\mathbf{s}(n)=[u(n), v(n)]$, where n is the index of the contour point, $1 \leqslant n \leqslant N$. The contour globally deforms to the expected location by minimizing an energy function consisting of internal energy and external energy. More details of snake technique can be found in Refs. [23,24]. A dynamic ρ–θ polar coordinate system of the optic disk is set up for contour deformation. The disk center is set to be the initial origin. Circular Hough transformation is first applied on the edge map of the optic disk image to obtain the best fitting circle with center $\bar{\mathbf{c}}_0$ and radius $\bar{r}$. The initial contour points are selected at $\rho = \bar{r}$ for every 5° of θ, resulting in $N = 72$ contour points. The contour deformation is made possible only along $\pm\rho$ directions. In the proposed method, the energy function is composed of four terms that are proportional to smoothness, gradient magnitude, gradient orientation, and intensity, all of which are written as

$$E(ni) = \beta_1 E_{smooth}(ni) + \beta_2 E_{gradient}(ni) + \beta_3 E_{orientation}(ni) + \beta_4 E_{intensity}(ni). \quad (1)$$

where ni is the candidate pixel. The new contour point n is set to be the candidate pixel with the lowest local energy.

In the energy function, the smoothness term is the summation of the absolute value of the first and second derivatives, which is similar to the internal energy of the original snake, written as

$$E_{smooth}(ni) = \alpha_1 \left| \frac{\mathrm{d}\mathbf{s}(ni)}{\mathrm{d}n} \right| + \alpha_2 \left| \frac{\mathrm{d}^2\mathbf{s}(ni)}{\mathrm{d}n^2} \right|, \quad (2)$$

where α_1 and α_2 are constants specifying the elasticity and stiffness of the snake, with α_2 set at 0.1 time of α_1 in this paper.

Magnitude of gradient, $E_{gradient}(ni) = -|\nabla I(ni)|$, can efficiently provide the boundary location. Gradient orientation is also considered in the energy function to make it robust to disturbance of the vessel edge. Let $Ori(n)$ denote the gradient orientation of the disk boundary at point n. Considering the optic disk is close to a circular shape and

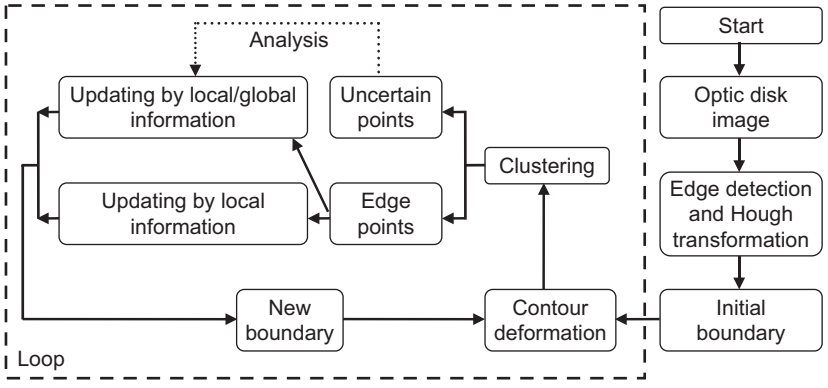

Fig. 2. Flowchart of optic disk boundary detection.

Please cite this article as: J. Xu, et al., Optic disk feature extraction via modified deformable model technique for glaucoma analysis, Pattern Recognition (2006), doi: 10.1016/j.patcog.2006.10.015

the disk region is brighter than the other region, the gradient orientation of the disk boundary at point n should be close to the angle of this point, θ_n. Hence, the gradient orientation term of the energy is written as

$$E_{orientation}(ni) = |Ori(ni) - \theta_n|. \quad (3)$$

On the disk boundary, most contour points have similar intensity value. Let T_{median} be the median intensity of the contour points and *Int(ni)* be the intensity value of individual candidate pixel. The absolute intensity difference is another term of the energy function:

$$E_{intensity}(ni) = |Int(ni) - T_{median}|. \quad (4)$$

Therefore, the total energy function of the candidate point ni can be written as

$$E(ni) = \beta_1 \left\{ \left| \frac{d\mathbf{s}(ni)}{dn} \right| + 0.1 \left| \frac{d^2\mathbf{s}(ni)}{dn^2} \right| \right\} + \beta_2\{-|\nabla I(ni)|\} + \beta_3|Ori(ni) - \theta_n| + \beta_4|Int(ni) - T_{median}|, \quad (5)$$

where β_1–β_4 are the weights of the energy terms. They may be set to the same value by default.

2.2. Parameter setting

Properly selecting parameters of the energy function is one important topic in snake technique. In this paper, to guarantee that each term contributes the same magnitude of energy, every term in the energy function is first normalized to the same range, such as [0, 1]. Then the weight parameter of each term could be set based on its level of importance in the whole energy function. They may also be set to the same value by default. Considering that the gradient magnitude and gradient orientation are more important features, their weight parameter values can be set slightly higher than the others. For example, $\beta_1 : \beta_2 : \beta_3 : \beta_4$ may be set as 1:1.2:1:1. The proposed method is not sensitive to the reasonable variation of weight ratio between each term.

2.3. Knowledge-based clustering of the contour points

In each iteration, the contour points deform to the locations with minimal combined energies. However, the deforming-only process could not give sufficient good contour result. Some points may not be located on the true edges of optic disk because of the effects of blood vessels, noises, ill-defined edges, etc. Hence the contour points are classified into uncertain-point group and edge-point group. The two groups are then updated using different operations. Precise classification is not necessary in this algorithm, because this is an iterative-update algorithm; the resulted contour does not only depend on one classification in an iteration. A simple and fast classification technique should be considered, since classification process is embedded into each iteration. The effect of the classification in the proposed method is that in each iteration, the points in certain proportion of the whole contour points (uncertain points), being most similar to false edge points, are classified and updated by global/local information; whereas the other points (edge points) are updated by local information only.

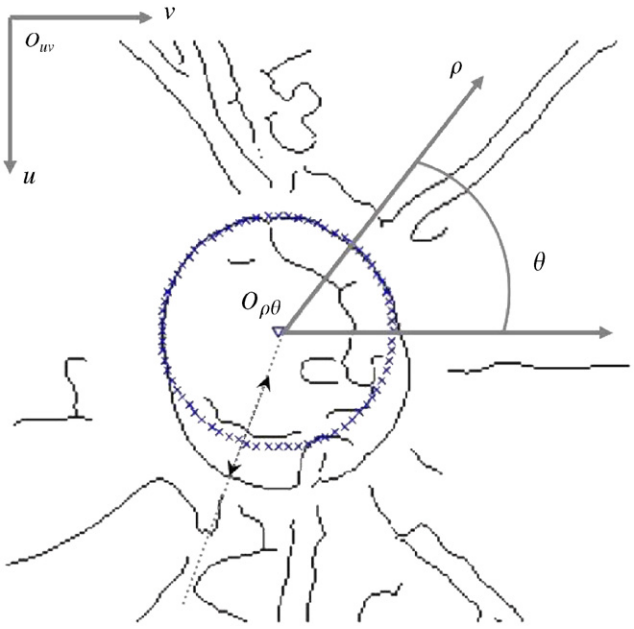

Fig. 3. An example of Hough transformation on edge map. Solid line is the edges; '∇'denotes initial disk center $\bar{\mathbf{c}}_0$; '×' indicates initial contour points based on $\bar{r}$.

Supervised learning is not suitable because the variations of the retinal color, fundus tissue reflection, and uneven photographic illumination in each fundus image makes it difficult to select a fix training set and estimate certain criterion to consistently classify the edge points and the uncertain points in different images. In this classification problem, it has been known that there are basically two classes. Hence, the simple unsupervised learning method, i.e., modified k-means algorithm, is sufficient to approximately group the contour points into two clusters, i.e., edge-point cluster and uncertain-point cluster. k-means algorithm uses sample properties extracted from single image to separate them through self-learning which is robust to the illumination changes and to the different tissue reflection from different eye images, etc.

The clustering samples are the intensity distribution of each contour point (ρ_n, θ_n) along radial line in the range of $\rho_n \pm \Delta_\rho$ pixels, as shown by the dash line with arrows in Fig. 3. Let $\mathbf{z}_n$ denote the sample vector, which must be normalized before clustering computation to enhance the weak edge. If the contour point is located on the disk edge, its intensity distribution will be similar to a negative-step profile as shown in Fig. 4(a). On the contrary, if the contour point is located on the blood vessel, disk region, or background region, it will have different distribution as shown in Fig. 4(b), (c). The proposed knowledge-based clustering

Please cite this article as: J. Xu, et al., Optic disk feature extraction via modified deformable model technique for glaucoma analysis, Pattern Recognition (2006), doi: 10.1016/j.patcog.2006.10.015

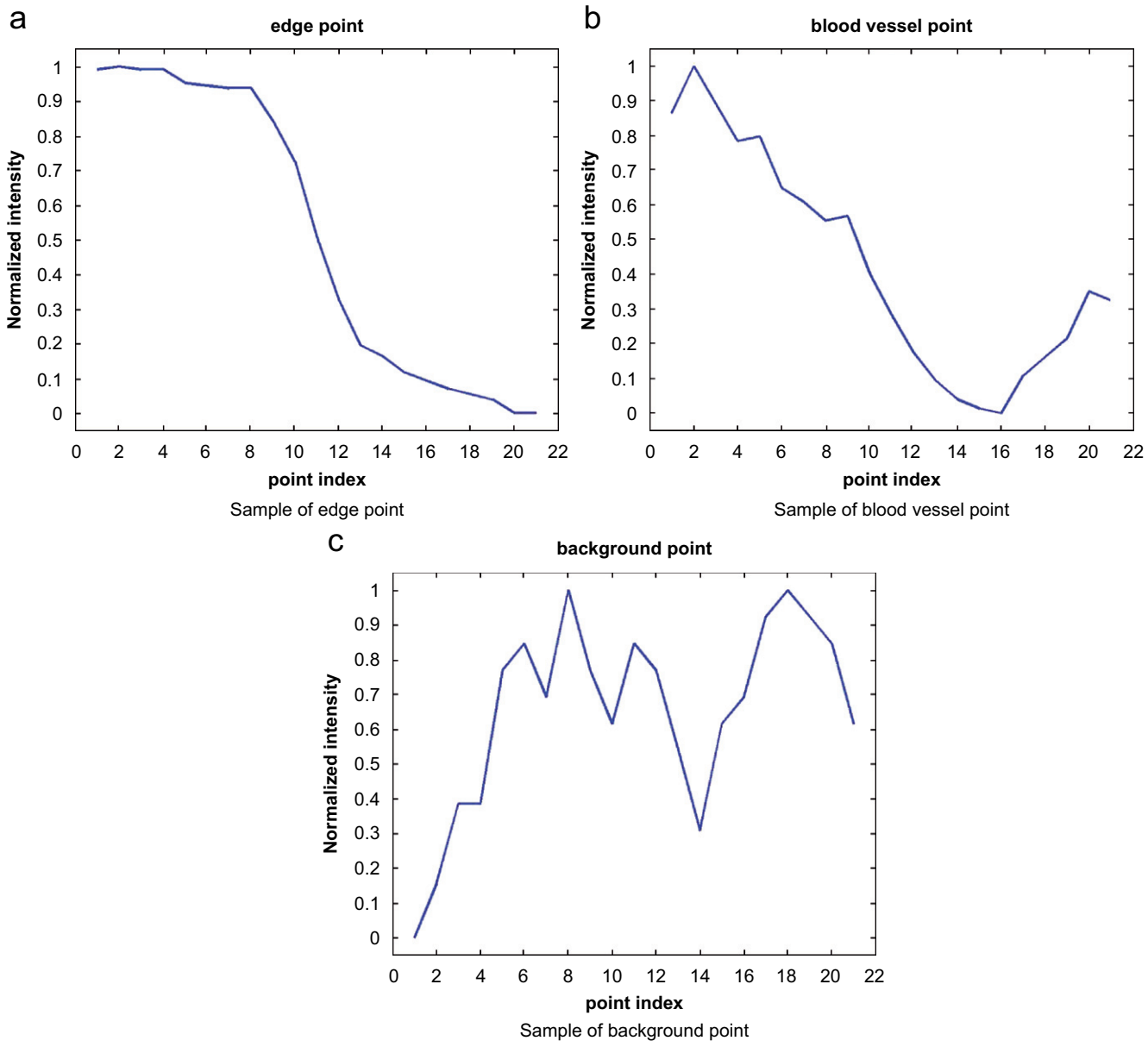

Fig. 4. Normalized clustering samples: (a) sample of edge point; (b) sample of blood vessel point; (c) sample of background point.

method is based on the assumption that more than 50% contour points are edge points. Then two features are extracted from the profile distributions of the samples for classification, based on the median of samples and the standard deviation of each sample, denoted by $\mathbf{fz}_n = [Dz_0(n), Pstd(n)]^{\mathrm{T}}$. The first feature is set to be $Dz_0(n) = \|\mathbf{z}_n - \mathbf{z}_0\|$, where $\mathbf{z}_0$ is the median vector of all the sample vectors $\mathbf{z}_n$, $n = 1, 2 \ldots 72$. The second feature is set to be the standard deviation of each sample vector, denoted as $Pstd(n) = std(\mathbf{z}_n)$. Then, the sample points are self-grouped into two clusters in the feature space.

Let S_1 and S_2 denote the edge-point cluster and the uncertain-point cluster, respectively. The contour points are classified into these two clusters by weighted k-means algorithm. At tth iteration, the sample $\mathbf{fz}_n$ is distributed among two clusters $\{S_1(t), S_2(t)\}$ according to the following rule:

$$\begin{cases} \mathbf{fz}_n \in S_1(t) & \text{if } \|\mathbf{fz}_n - \mathbf{c}_1\| \leqslant wm\|\mathbf{fz}_n - \mathbf{c}_2\|, \\ \mathbf{fz}_n \in S_2(t) & \text{if } \|\mathbf{fz}_n - \mathbf{c}_1\| > wm\|\mathbf{fz}_n - \mathbf{c}_2\|, \end{cases} \tag{6}$$

where wm is the weight used to adjust the number of samples in each class, $\mathbf{c}_1$ and $\mathbf{c}_2$ are cluster centers, which are then updated by

$$\mathbf{c}_j(t+1) = \frac{1}{|S_j|} \sum_{\mathbf{fz}_n \in S_j(t)} \mathbf{fz}_n, \quad j = 1, 2, \tag{7}$$

Please cite this article as: J. Xu, et al., Optic disk feature extraction via modified deformable model technique for glaucoma analysis, Pattern Recognition (2006), doi: 10.1016/j.patcog.2006.10.015

where $|S_j|$ is the sample number in cluster j. The clustering iteration will stop, if both of two cluster centers do not change in the iteration. Because the following smoothing update is based on the information of S_1 (edge-point cluster), the sample number in S_1 should dominate, i.e., $|S_1| > |S_2|$. Hence a weight wm is introduced in the k-means algorithm as shown in Eq. (6) to adjust the distribution of the sample numbers in two clusters. $|S_1|$ can be guaranteed to be in the range of $[N_{Low}, N_{High}]$ by self-adjusting the weight wm. If $N_1 < N_{Low}$, wm is increased; and if $N_1 > N_{High}$, wm is decreased. N_{Low} and N_{High} are set based on the medical background knowledge that approximately 20% contour points are the blood vessel points.

2.4. Smoothing update

After contour deformation and clustering, edge-point cluster and uncertain-point cluster are obtained. The points belonging to different clusters are updated by different criteria. This operation will retain the edge points close to their original positions and update the uncertain points to the correct positions. All the contour points, whether they are in S_1 or S_2, are updated using the information of their neighbors in S_1. The point information in S_2, however, is not used for update. Each point's radius ρ_n is updated by its neighboring edge points while keeping the angle θ_n fixed. The number of neighbors used for updating denoted as $win(n)$ is varied based on the analyzed result of its neighbors. An example is illustrated in Fig. 5(a) to explain the smoothing update, where $win(n)$ is set to be 2, the '×' points are the edge points belonging to S_1, and the 'o' points indicate the uncertain points belonging to S_2. The radius ρ_n of point n is replaced by the average value of its first and second closest neighboring edge points ('×' points) in S_1 along both $\pm\Delta\theta_n$ sides, written as

$$\rho_n^{update} = average\{\rho_{nl_1}, \rho_{nl_2}, \rho_n, \rho_{nr_1}, \rho_{nr_2}\}, \quad (8)$$

where nl_2, nl_1, nr_1, nr_2 are the first and second closest '×' points to point n along $\pm\Delta\theta_n$ directions. If point n is the uncertain point, it is not used in Eq. (8) for updating computation.

The updating sample number of neighbors $win(n)$ is varied for different contour point based on the information analyzed from the neighbors. The uncertain-point cluster S_2 consists of points belonging to vessels or noises. The vessel points tend to scatter on the whole contour and generally have only several continuous points as shown by the circle points in Fig. 5(a). The noise points are arbitrarily located anywhere on the contour. In some cases, the noise points occur almost continuously in certain large region, as shown by the circle points in Fig. 5(b). Small $win(\bullet)$, such as $win(\bullet) = 2$, only uses the local information to update the contour point. It is able to solve the problem of blood vessel occlusion as shown in Fig. 5(a), while the original positions of the correct edge points are approximately maintained.

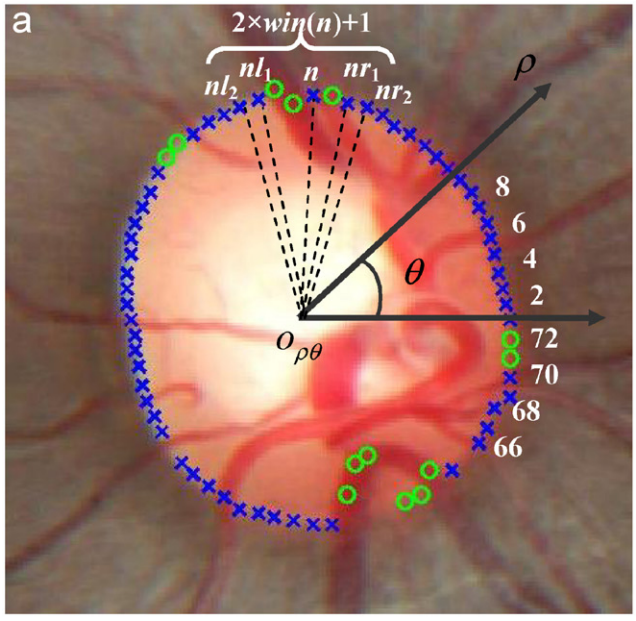

Dispersedly uncertain points

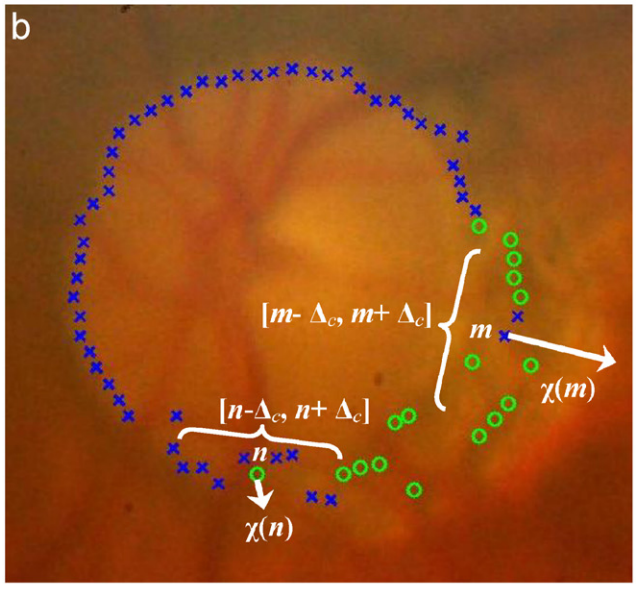

Continuously uncertain points.

Fig. 5. Clustered contour points. '×'—edge points; 'o' —uncertain points: (a) dispersedly uncertain points; (b) continuously uncertain points.

However, if the contour has continuously uncertain points as shown in Fig. 5(b), small $win(\bullet)$ may not provide reliable boundary points. Hence, $win(\bullet)$ should be increased in the continuous noise region, where the updating is based on semi-global information, or even global information when $win(\bullet)$ increases to the half of the whole contour. Global information therefore helps restrict the contour within certain model, whereas local information provides the detailed variation of the contour. Therefore, variable updating sample number for different contour points can balance the stability and accuracy of the contour.

Please cite this article as: J. Xu, et al., Optic disk feature extraction via modified deformable model technique for glaucoma analysis, Pattern Recognition (2006), doi: 10.1016/j.patcog.2006.10.015

For every contour point n, the *combination force* $\boldsymbol{\chi}(n)$ of the neighbors within the range of $[n-\Delta_c, n+\Delta_c]$ is used to set the updating sample number $win(n)$. $\boldsymbol{\chi}(n)$ is computed as

$$\chi(n) = \sum_i w_i Norm_i, \quad i \in [n-\Delta_c, n+\Delta_c],$$
$$w_i = \begin{cases} 0 & \text{if } \boldsymbol{n} \in S_1, \\ 1 & \text{if } \boldsymbol{n} \in S_2, \end{cases} \tag{9}$$

where $Norm_i$ is the unit orientation vector of the contour point i, denoted as $Norm_i = (\cos(\theta_i), \sin(\theta_i))$. The weights w_i is set to be 0 for edge point and 1 for uncertain point, respectively. Small $\|\boldsymbol{\chi}(n)\|$ indicates blood vessel region or small noise region, and large $\|\boldsymbol{\chi}(n)\|$ denotes the continuation of uncertain noise region as shown in Fig. 5(b). Therefore $win(n)$ is set to linearly increase based on the increase of $\|\boldsymbol{\chi}(n)\|$, written as

$$win(n) = \begin{cases} 2 & \text{if } \|\boldsymbol{\chi}_{win}(n)\| \leqslant 5, \\ 2 + (\|\boldsymbol{\chi}_{win}(n)\| - 5) & \text{if } \|\boldsymbol{\chi}_{win}(n)\| > 5. \end{cases} \tag{10}$$

Variable updating sample numbers let the smoothing update auto-adjust between global and local information. Hence, for the large uncertain noise region, the contour is updated based on the information of the global model; on the contrary, for the certain disk-edge region, the contour is retained close to its original points.

2.5. Stop criterion

After contour deformation, clustering and updating, the new contour is obtained. The origin of the ρ–θ polar coordinate system shifts to the centroid of new contour after each iteration. The average deforming distance in each iteration is used to set the stopping criterion. At iteration t, the average absolute distance (AAD) between the old contour and deformed contour is defined as

$$AAD(t) = \frac{1}{N}\sum_{n=1}^{N} \|\mathbf{s}^t(n) - \mathbf{s}^{t-1}(n)\|. \tag{11}$$

The operation is repeated, until the AAD is less than 1 pixel for five consecutive iterations.

2.6. Evaluation

The ground truth of the boundary is manually labeled under the supervision of ophthalmologists. The average distance from the detected boundary point to the ground truth is measured for evaluation. The ground truth, denoted by A, consists of the individual pixel a_i, $1 \leqslant i \leqslant M$, where M is the amount of the pixel on the ground truth boundary. $\hat{\mathbf{s}}(n) = [u(n), v(n)]$ is the final contour, $1 \leqslant n \leqslant N$. For each contour point n, the distance to the closest point (DCP) of ground truth is defined as

$$DCP(\hat{\mathbf{s}}(n), A) = \min \|\hat{\mathbf{s}}(n) - a_i\|, \quad 1 \leqslant i \leqslant M. \tag{12}$$

The accuracy of the detected boundary is evaluated by the mean of DCP (MDCP) as follows:

$$MDCP(\hat{\mathbf{s}}, A) = \frac{1}{N}\sum_{n=1}^{N} DCP(\hat{\mathbf{s}}(n), A). \tag{13}$$

The smaller MDCP is, the closer the detected boundary is to the ground truth.

3. Cup boundary detection

The available 3-D optic disk image and disk boundary are the preconditions to estimate the cup boundary. Then the clinical disk parameters could be obtained from the detected disk and cup boundaries for analysis, diagnosis, and monitoring. Fig. 6 gives the basic steps of disk parameter estimation. Compared with the disk boundary detection on the 2-D fundus image, the variable shapes and colors of cup make it more difficult to be automatically segmented. Moreover, in many images, the cup contour could not be easily measured even manually without some experience. Hence, automated detection of cup boundary is a challenging task in fundus image processing.

3-D optic disk image is necessary in cup boundary detection, which is obtained from the prior published work [25]. The modified deformable model technique described in Section 2 is applied to extract the cup boundary by using a different energy function. The origin of ρ–θ polar coordinate system is initialized at the center of the detected disk boundary. The initial cup points are set to the locations where the disk points are shrunk by 10 pixels toward the origin written as

$$\rho_n^{initial\ cup} = \rho_n^{disk} - 10 \text{ pixels}, \quad 1 \leqslant n \leqslant N. \tag{14}$$

The energy function that fuses together the information of depth, gradient, smoothness, and shape, is written as

$$Ecup(ni) = \lambda_1 E_{depth}(ni) + \lambda_2 E_{gradient}(ni) + \lambda_3 E_{smooth}(ni) + \lambda_4 E_{shape}(ni), \tag{15}$$

where depth and gradient terms give local information, whereas the shape term provides the global information of cup shape so as to make the contour deformation more reliable. λ_1–λ_4 are the weights for each energy term.

Let d_n be the depth of each optic disk point and $d(ni)$ be the depth of each candidate pixel. Here cup boundary is defined at the location of $\frac{1}{3}$ down from each point of the

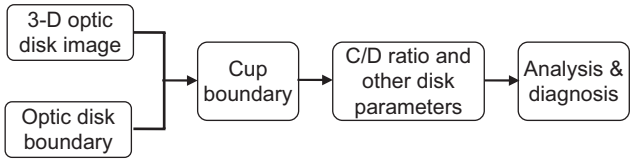

Fig. 6. Flowchart of disk parameter estimation.

Please cite this article as: J. Xu, et al., Optic disk feature extraction via modified deformable model technique for glaucoma analysis, Pattern Recognition (2006), doi: 10.1016/j.patcog.2006.10.015

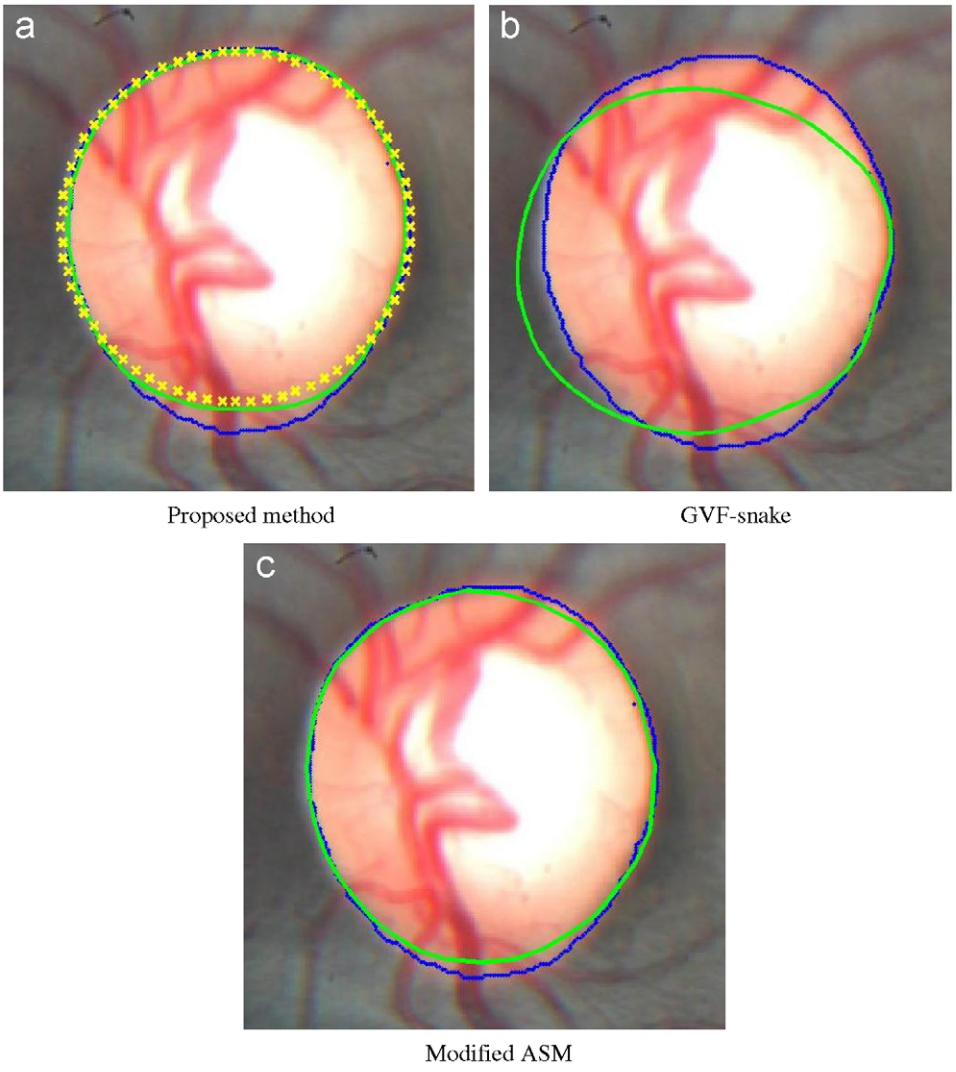

Fig. 7. An example of common elliptic optic disk. '×' indicates initial contour points; dark contour is the ground truth; bright line is resulted contour: (a) proposed method; (b) GVF-snake; (c) modified ASM.

disk boundary to the deepest disk point d_{min}, denoted as $\Delta_n = (d_n - d_{min})/3$. Then the depth term of the energy is

$$E_{depth}(ni) = |d(ni) - \Delta_n|. \tag{16}$$

Gradient is useful information, if there is pallor in the optic disk. Gradient term consists of both gradient magnitude $\nabla I(ni)$ and gradient orientation $Ori(ni)$ as

$$E_{gradient}(ni) = -|\nabla I(ni)| + |Ori(ni) - \theta_n|. \tag{17}$$

The definitions of $\nabla I(ni)$ and $Ori(ni)$ are the same as the ones introduced in Section 2.

The internal energy of the contour is set to be the smoothness term of the energy, where the coefficient of the second derivative is set to be 0.5 time of the first derivative.

$$E_{smooth}(ni) = \left|\frac{\mathrm{d}\mathbf{s}(ni)}{\mathrm{d}n}\right| + 0.5 \times \left|\frac{\mathrm{d}^2\mathbf{s}(ni)}{\mathrm{d}n^2}\right|. \tag{18}$$

The free-form deformation may give uncertain shape if the cup features are not obvious. Therefore shape model is introduced in the energy function to constrain the deformation to be close to certain predefined shape. Let $\mathbf{s}^{shape}$ be the shape model of the cup, which is expressed in ρ–θ coordinate system as $\mathbf{s}^{shape}(n) = [\rho_n^{shape}, \theta_n^{shape}]$, $1 \leqslant n \leqslant N$. The shape model could be estimated from training set, or set to be an ellipse (or circle). In this paper, the disk shape is used as the shape model for cup contour deformation. The shape term of the energy is set to be the radial distance between the candidate pixel and the model pixel as given by

$$E_{shape}(ni) = |\rho_{ni} - \rho_n^{shape}|, \tag{19}$$

where the candidate points close to the shape model have low energy, and the points far away from the shape model have high energy.

Please cite this article as: J. Xu, et al., Optic disk feature extraction via modified deformable model technique for glaucoma analysis, Pattern Recognition (2006), doi: 10.1016/j.patcog.2006.10.015

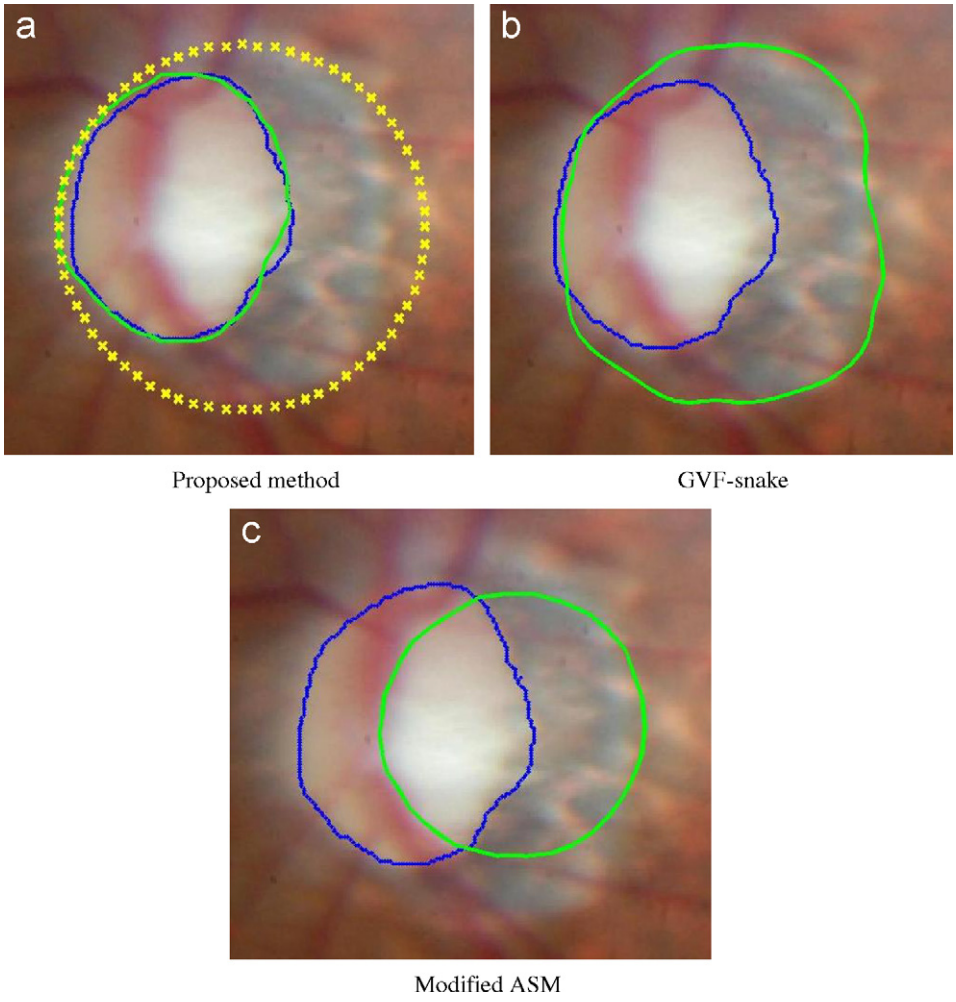

Fig. 8. An example of ill-defined optic disk boundary. '×' indicates initial contour points; dark contour is the ground truth; bright line is resulted contour: (a) proposed method; (b) GVF-snake; (c) modified ASM.

The full energy function is written as

$$\begin{aligned} &Ecup(ni) \\ &= \lambda_1 |d(ni) - \Delta_n| + \lambda_2 \{-|\nabla I(ni)| + |Ori(ni) - \theta_n|\} \\ &\quad + \lambda_3 \left\{ \left| \frac{\mathrm{d}\mathbf{s}(ni)}{\mathrm{d}n} \right| + 0.5 \times \left| \frac{\mathrm{d}^2\mathbf{s}(ni)}{\mathrm{d}n^2} \right| \right\} \\ &\quad + \lambda_4 \left| \rho_{ni} - \rho_n^{shape} \right|. \end{aligned} \tag{20}$$

In each iteration, the shape model is first aligned based on the cup contour obtained from previous iteration, and then the cup contour deforms to the location where the combined energies of depth, gradient, smoothness, and shape are smallest, finally the contour points are classified and updated. The deformation will stop, when the average contour variation is less than 1 pixel for five consecutive iterations.

4. Results

4.1. Results of disk boundary detection and evaluation

One hundred fundus images provided by the National University Hospital were tested by the proposed modified deformable model method, where the weight ratio was set to be $\beta_1 : \beta_2 : \beta_3 : \beta_4 = 1 : 1.2 : 1 : 1$. The results were then compared with GVF-snake [6] and modified ASM algorithm [13,14] based on the same initial boundary. In the modified ASM algorithm, PCA based method for disk center localization was also used, but it did not improve the accuracy of final disk boundary compared with the result from disk center estimated by circular Hough transformation. In GVF-snake, the images were preprocessed by morphological operation; and the parameters in the energy functions were carefully set to make a balance between the smoothness and the accuracy on the resulted boundary. The disk boundary manually marked by the experienced ophthalmologist was set to be the ground truth. Then MDCP was measured to evaluate the accuracy of the detected boundary.

An example of common elliptic optic disk is illustrated in Fig. 7, where both the proposed method and ASM method give the successful results, GVF snake gives the failed result. The measured MDCPs are, respectively, 1.6, 6.2 and 1.6 pixels for the proposed method, GVF-snake and the modified ASM.

Please cite this article as: J. Xu, et al., Optic disk feature extraction via modified deformable model technique for glaucoma analysis, Pattern Recognition (2006), doi: 10.1016/j.patcog.2006.10.015

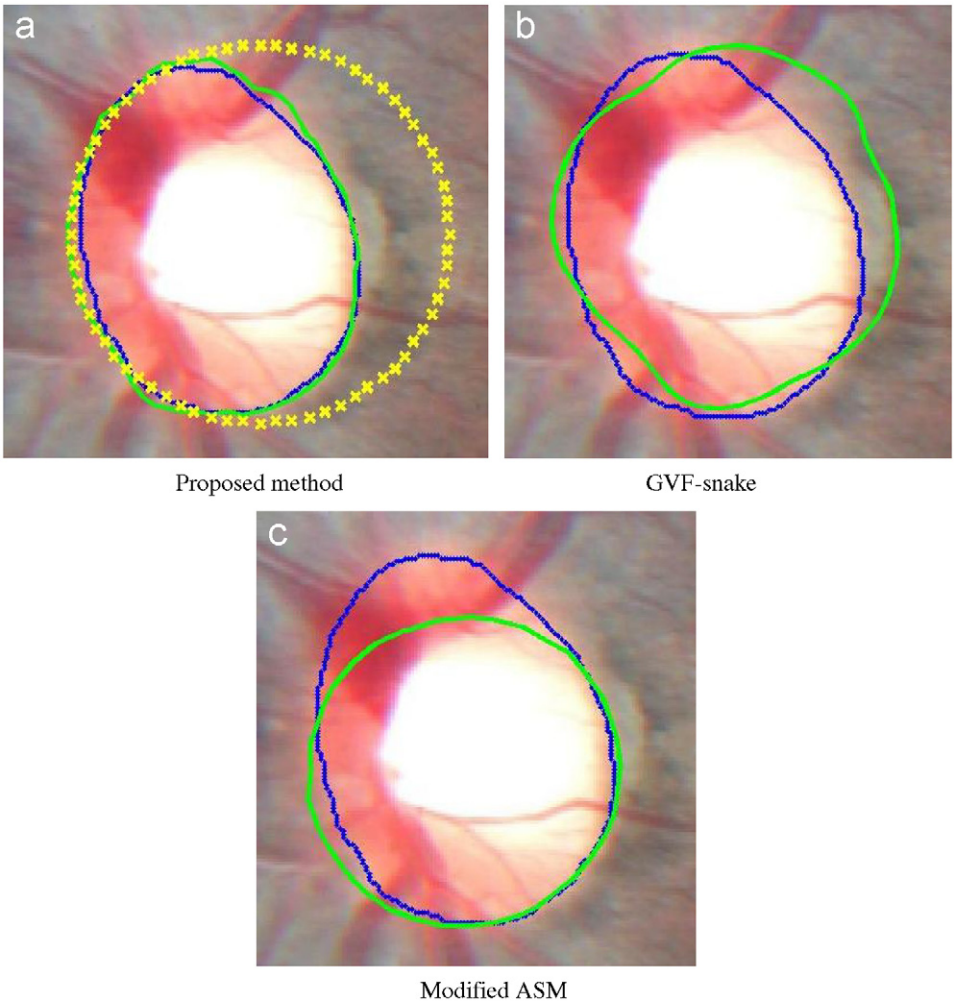

Fig. 9. An example of fuzzy elliptic optic disk. '×' indicates initial contour points; dark contour is the ground truth; bright line is resulted contour: (a) proposed method; (b) GVF-snake; (c) modified ASM.

The example given in Fig. 8 is a small optic disk with ill-defined boundary and noises from the surrounding tissue which make the initial contour far away from the real boundary. The initial disk contour was estimated by circular Hough transformation in the edge map, as shown by '×' in Fig. 8(a). The final boundary was then obtained through contour deformation, clustering, and updating, as given in Fig. 8(a), where the bright line is the final disk boundary and the dark line is the ground truth manually placed by ophthalmologist. The GVF-snake and modified ASM were both applied on this example under the same initial circular contour for comparison and the results are given in Fig. 8(b), (c). The measured MDCPs are, respectively, 2.4, 23.6 and 24.2 pixels for the proposed method, GVF-snake and the modified ASM. The proposed methods correctly located the disk boundary, while both the GVF-snake and modified ASM method failed.

One more example of fuzzy elliptic optic disk is illustrated in Fig. 9(a). The MDCP was measured to be 1.9 pixels in this example. The resulted boundaries for GVF-snake and modified ASM are given in Fig. 9(b), (c), in which the MDCPs are 6.7 and 3.5 pixels, respectively. It can be obviously seen that the proposed method provides better result.

The failure case due to wrongly estimating the disk center under the disturbance of large bright lesion is shown in Fig. 10. In this example, PCA based approach [4] was employed in modified ASM method to identify disk center; however, neither can it locate the disk center correctly. Three different methods were applied on this image and all of them failed.

Table 1 shows the statistical comparison among the proposed method, GVF-snake and the modified ASM, where $\mathrm{MDCP} \leqslant 3$ pixels indicates success, $3 < \mathrm{MDCP} \leqslant 5$ pixels denotes a fair result requiring improvement, and $\mathrm{MDCP} > 5$ pixels means a failure. Among the 100 testing images operated by the proposed method, 94 images were successfully processed; five images required further improvement and one image failed. It can be observed that the ASM method is much better than GVF-snake. Compared with the "smart" method, the average numbers of iterations are 8.8 and

Please cite this article as: J. Xu, et al., Optic disk feature extraction via modified deformable model technique for glaucoma analysis, Pattern Recognition (2006), doi: 10.1016/j.patcog.2006.10.015

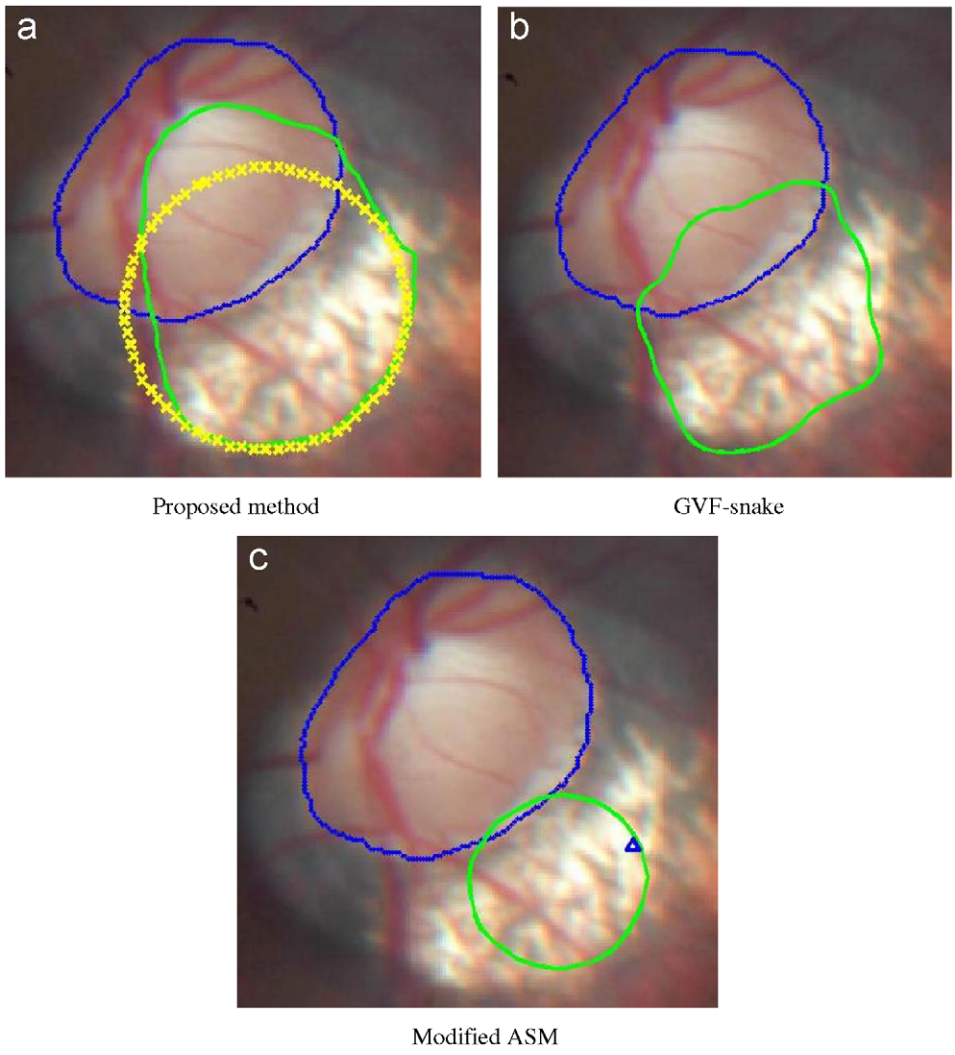

Fig. 10. A failure example due to lesion disturbance on disk edge. '×' indicates initial contour points; dark contour is the ground truth; bright line is resulted contour; 'Δ' is the disk center from PCA: (a) proposed method; (b) GVF-snake; (c) modified ASM.

Table 1
Comparison of mean distance to closest point (MDCP) among different methods

Method	Result		
	Proposed method	GVF-snake	Modified ASM
Success (MDCP <3 pixels)	94	12	82
Fair (MDCP $=3$–5 pixels)	5	33	9
Fail (MDCP $\geqslant 5$ pixels)	1	55	9
Success (%)	94	12	82
Mean MCDP of success (pixels)	1.3	3.6	1.8
STD of MDCP of success (pixels)	0.51	0.60	0.54

34.1, and the average computational time are 7.5 and 8.2 s, respectively, for the proposed method and ASM method, respectively. Accordingly, the proposed method achieved more successful number of results; and also obtained more accurate boundaries in the successful cases than the other two methods.

To show the stability of the proposed method, the weight ratio of energy function was changed into different values and were applied on the same 100 testing images. As described in Section 2.2, based on the knowledge that the weights of gradient magnitude (β_2) and gradient orientation (β_3) should be set to be slightly higher than the other

Please cite this article as: J. Xu, et al., Optic disk feature extraction via modified deformable model technique for glaucoma analysis, Pattern Recognition (2006), doi: 10.1016/j.patcog.2006.10.015

weights, β_1 and β_4 were fixed at 1; β_2 and β_3 were varied in the range of [1,2]. The results of five different settings are listed in Table 2. The mean and standard deviation of the success rate were measured to be 93% and 0.8%, respectively, and the mean MDCP of successful cases were all 1.3 pixels for these five settings; thus it showed that the proposed method was not sensitive to the reasonable variation of weight ratio.

Table 2
Results of variable weight ratio of the proposed method

No.	Weight ratio of energy function $\beta_1:\beta_2:\beta_3:\beta_4$	Success (%)	Mean MDCP of success (pixel)
1	1:1.2:1.0:1	94	1.3
2	1:1.2:1.2:1	93	1.3
3	1:1.5:1.2:1	94	1.3
4	1:1.0:1.0:1	92	1.3
5	1:1.6:1.3:1	94	1.3
Mean	—	93	1.3
STD	—	0.8	0

STD denotes standard deviation.

4.2. Results of cup boundary detection and evaluation

In the 100 testing images mentioned in Section 4.1, Twenty-five of them have corresponding HRT results. The proposed method of cup boundary detection was employed on these 25 images and then the results were compared with HRT results. In HRT system, the disk contour was manually placed by the clinicians first, and then the system generated the cup contour based on the labeled disk contour and the depth information from the 3-D HRT image.

One example of obvious pallor in the optic disk is illustrated in Fig. 11(a), compared with HRT result in Fig. 11(b), where the outer contour is the disk boundary and the inner contour is the cup boundary. The ground truth was labeled by the experienced ophthalmologist as given in Fig. 11(c). Since the automated estimation of the cup contour is still a challenging work, it can be noticed that the cup contours are not exactly the same as the ground truth, but they have similar shape. The C/D ratio is not only a useful disk parameter for analysis, but also for evaluating the results of the estimated cup boundary. The contours estimated by the ophthalmologist were set to be the ground truth.

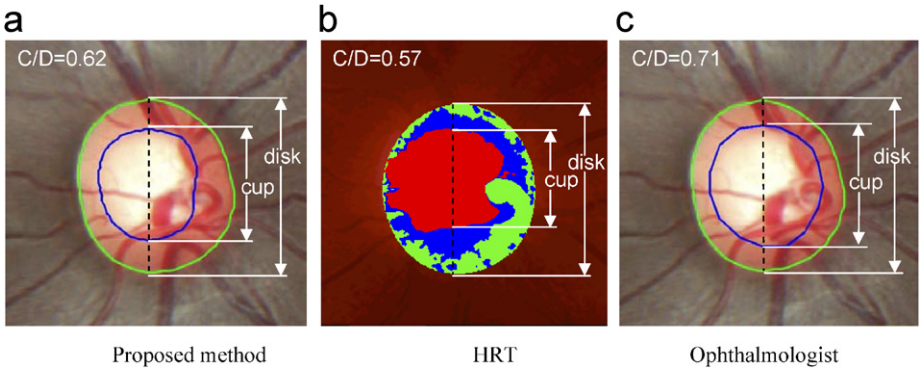

Fig. 11. An example of optic disk with obvious pallor: (a) proposed method; (b) HRT; (c) ophthalmologist.

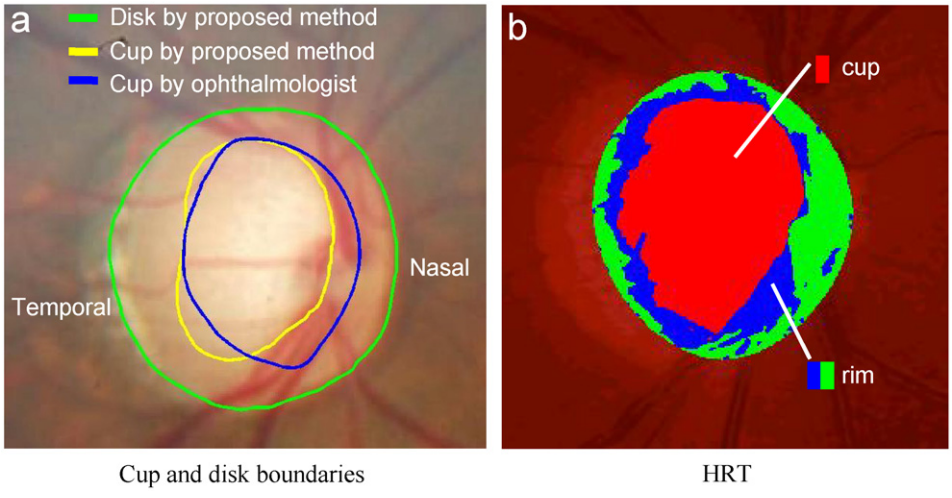

Fig. 12. Another example of optic disk with non-obvious pallor: (a) cup and disk boundaries; (b) HRT.

Please cite this article as: J. Xu, et al., Optic disk feature extraction via modified deformable model technique for glaucoma analysis, Pattern Recognition (2006), doi: 10.1016/j.patcog.2006.10.015

Table 3
Cup-to-disk (C/D) vertical ratio

No.	Proposed method	HRT	Ophthalmologist
1	0.59	0.58	0.54
2	0.49	0.66	0.72
3	0.65	0.63	0.66
4	0.56	0.61	0.67
5	0.64	0.45	0.52
6	0.66	0.46	0.69
7	0.82	0.94	0.85
8	0.70	0.21	0.76
9	0.68	0.82	0.78
10	0.73	0.79	0.77
11	0.59	0.41	0.48
12	0.47	0.37	0.52
13	0.45	0.27	0.44
14	0.43	0.46	0.52
15	0.70	0.47	0.65
16	0.61	0.69	0.70
17	0.78	0.88	0.82
18	0.70	0.86	0.65
19	0.61	0.76	0.72
20	0.72	0.78	0.73
21	0.58	0.60	0.68
22	0.66	0.58	0.62
23	0.62	0.58	0.72
24	0.67	0.56	0.68
25	0.62	0.57	0.71
Correlation	0.71	0.67	—

The C/D vertical ratios were measured to be 0.62, 0.57, and 0.71 from the proposed method, HRT, and an ophthalmologist, respectively.

Another example of non-obvious pallor is shown in Fig. 12(a). The bending of small vessels is obvious at temporal side in this example. The corresponding HRT result is given in Fig. 12(b), where the cup is estimated only based on the depth information in HRT. It can be observed that the boundary placed by the ophthalmologist and the boundary estimated by the proposed method are close at temporal side. However, the two boundaries at the nasal side are slightly different, because there is no obvious cup feature on nasal side, and also the main blood vessels occlude on that region. Hence, it is difficult to decide the exact location of cup edge on the nasal side in this example. The C/D vertical ratios were measured to be 0.71, 0.78, and 0.73 from the proposed method, HRT, and an ophthalmologist, respectively.

The C/D vertical ratios of 25 testing images were computed and given in Table 3. The correlations of the results with ground truth are 0.71 and 0.67, respectively, for the proposed method and HRT. It implies the proposed method of cup boundary estimation gives results comparable with those from HRT.

5. Conclusion

Reliable and fully automated extraction of optic disk parameters can be a valuable diagnostic-assisting resource for clinicians. Much of prior work has focused on optic disk boundary detection, however the vessel occlusion problem has not been well solved. The present work has made a few contributions by proposing a novel approach to disk boundary detection which directly solves the problem of blood vessel occlusions. The method is then extended to detect the cup boundary and estimate the clinical disk parameter. The contour is initialized by Hough transformation in edge map, and then processed by contour deformation, knowledge-based clustering, and updating. Clustering operation can perform self-grouping of contour points into uncertain-point cluster and edge-point group based on the knowledge in the extended area of the contour. The updating sample number is self-adjusted and combines both the global and local information to update the contour points after each radial deformation. These modifications make the proposed approach robust to blood vessel occlusions, ill-defined edges, fuzzy shapes and noises, while maintaining the accuracy.

The experimental results show that 94% disk boundaries can be measured successfully by the proposed method out of 100 testing images. It turns out to be more robust and accurate than GVF-snake and modified ASM algorithm, from which the success rates are 12% and 82%, respectively. With the proper modification of energy function, the proposed method has been extended to detect the cup boundary. The estimated C/D ratios based on the detected cup and disk boundaries show good consistency and compatibility when compared with the results from HRT. Automated and quantitative extraction of optic disk parameter by the proposed method therefore can help clinicians implement more economical and conventional instrument modality in several eye-care applications, such as diagnosis, screening, and monitoring. Under proper modifications, the investigated method may also be applied to many other applications with similar problems, such as occlusions on object boundary.

6. Summary

The 3-D shape of the optic disk is an important indicator of various ophthalmic pathologies. Clinicians quantify the cupping of the optic disk to evaluate the progression of the eye disease, where cup is defined at certain depth down from the disk edges. Cup and disk boundaries act as the references to quantitative measurements of the disk parameters, such as cup-to-disk (C/D) vertical ratio, etc., which are the important parameters for diagnosis. Reliable and fully automated extraction of optic disk parameters can be a valuable diagnostic-assisting resource for clinicians. Much of prior work has focused on optic disk boundary detection, however the vessel occlusion problem has not been well solved. A novel deformable-model based approach is presented in this paper for robust detection of optic disk and cup boundaries. The method proposed here improves and extends the original snake, which is essentially a deforming-only technique, in two aspects: knowledge-based clustering and smoothing

Please cite this article as: J. Xu, et al., Optic disk feature extraction via modified deformable model technique for glaucoma analysis, Pattern Recognition (2006), doi: 10.1016/j.patcog.2006.10.015

update. The contour deforms to the location with minimum energy, and then self-clusters into two groups, i.e., edge-point group and uncertain-point group, which are finally updated by the combination of both local and global information. The modifications enable the proposed algorithm to become more accurate and robust to blood vessel occlusions, noises, ill-defined edges and fuzzy contour shapes. The experimental results show that 94% disk boundaries can be measured successfully by the proposed method out of 100 testing images. It turns out to be more robust and accurate than gradient vector flow snake (GVF-snake) and modified active shape model (ASM) algorithm, from which the success rates are 12% and 82%, respectively. With the proper modification of energy function, the proposed method is extended to detect the cup boundary and then extract the disk parameters for clinical application, which is a relatively new task in fundus image processing. The resulted C/D ratio shows good consistency and compatibility when compared with the results from Heidelberg Retina Tomograph (HRT) under clinical validation. Automated and quantitative extraction of optic disk parameter by the proposed method therefore can help clinicians implement more economical and conventional instrument modality in several eye-care applications, such as diagnosis, screening, and monitoring.

References

[1] C. Sinthanayothin, J.A. Boyce, H.L. Cook, T.H. Williamson, Automated localisation of the optic disc, fovea, and retinal blood vessels from digital colour fundus images, British J. Ophthalmol. 83 (1999) 902–910.
[2] S. Tamur, Y. Okamoto, Zero-crossing interval correction in tracing eye-fundus blood vessels, Pattern Recognition 21 (3) (1988) 227–233.
[3] A. Pinz, S. Bernogger, P. Datlinger, A. Kruger, Mapping the human retina, IEEE Trans. Med. Imaging 17 (1998) 606–619.
[4] H. Li, O. Chutatape, Automatic location of optic disk in retinal images, in: Proceedings of the International Conference on Image Processing, vol. 2, October 2001, pp. 837–840.
[5] M. Lalonde, M. Beaulieu, L. Gagnon, Fast and robust optic disc detection using pyramidal decomposition and Hausdorff-based template matching, IEEE Trans. Med. Imaging 20 (11) (2001) 1193–1200.
[6] A. Osareh, M. Mirmehd, B. Thomas, R. Markham, Comparison of colour spaces for optic disc localisation in retinal images, in: Proceedings of the 16th International Conference on Pattern Recognition, vol. 1, August 2002, pp. 743–746.
[7] J. Lowell, A. Hunter, D. Steel, A. Basu, R. Ryder, E. Fletcher, L. Kennedy, Optic nerve head segmentation, IEEE Trans. Med. Imaging 23 (2) (2004) 256–264.
[8] A. Hoover, M. Goldbaum, Locating the optic nerve in a retinal image using the fuzzy convergence of the blood vessels, IEEE Trans. Med. Imaging 22 (8) (2003) 951–958.
[9] M. Foracchia, E. Grisan, A. Ruggeri, Detection of optic disc in retinal images by means of a geometrical model of vessel structure, IEEE Trans. Med. Imaging 23 (10) (2004) 1189–1195.
[10] E. Trucco, P.J. Kamat, Locating the optic disk in retinal images via plausible detection and constraint satisfaction, in: Proceedings of the International Conference on Image Processing, October 2004, pp. 155–158 .
[11] F. Mendels, C. Heneghan, J.P. Thiran, Identification of the optic disc boundary in retinal images using active contours, in: Proceedings of the IMVIP Conference, 1999, pp. 103–115.
[12] T. Walter, J.C. Klein, P. Massin, A. Erginay, A contribution of image processing to the diagnosis of diabetic retinopathy-detection of exudates in color fundus images of the human retina, IEEE Trans. Med. Imaging 21 (10) (2002) 1236–1243.
[13] H. Li, O. Chutatape, Boundary detection of optic disk by a modified ASM method, Pattern Recognition 36 (9) (2003) 2093–2104.
[14] H. Li, O. Chutatape, Automated feature extraction in color retinal images by a model based approach, IEEE Trans. Biomed. Eng. 51 (2) (2004) 246–254.
[15] R. Malladi, J.A. Sethian, B.C. Vemuri, Shape modeling with front propagation: a level set approach, IEEE Trans. Pattern Anal. Mach. Intell. 17 (2) (1995) 158–175.
[16] E. Corona, S. Mitra, M. Wilson, T. Krile, Y.H. Kwon, P. Soliz, Digital stereo image analyzer for generating automated 3-D measures of optic disc deformation in glaucoma, IEEE Trans. Med. Imaging 21 (10) (2002) 1244–1253.
[17] Quantitative three-dimensional imaging of the posterior segment with the Heidelberg Retina Tomograph, HRT tutorial, ⟨http://www.heidelbergengineering.com/hrtf/hrt.html⟩, 2005.
[18] G.J. Jaffe, J. Caprioli, Optical coherence tomography to detect and manage retinal disease and glaucoma, Am. J. Ophthalmol. 137 (2004) 156–169.
[19] J. Caprioli, U. Klingbeil, M. Sears, B. Pope, Reproducibility of optic disc measurements with computerized analysis of stereoscopic video images, Arch. Ophthalmol. 104 (7) (1986) 1035–1039.
[20] U. Klingbeil, Fundus geometry measured with the analyzing stereo video ophthalmoscope, book chapter, internal circulation documents.
[21] R. Varma, G.L. Spaeth, The PAR IS-2000: a new system for retinal digital image analysis, Ophthalmic Surg. 19 (3) (1988) 183–192.
[22] P. Hrynchak, N. Hutchings, D. Jones, T. Simpson, A comparison of cup-to-disc ratio measurement in normal subjects using optical coherence tomography image analysis of the optic nerve head and stereo fundus biomicroscopy, Ophthal. Physiol. Opt. 24 (6) (2004) 543–550.
[23] M. Kass, A. Witkin, D. Terzopoulos, Snakes: active contour models, Int. J. Comput. Vision 1 (1987) 321–331.
[24] M. Sonka, V. Hlavac, R. Boyle, Imagep processing, analysis, and machine vision, PWS Publishing, Pacific Grove, CA, 1999.
[25] J. Xu, O. Chutatape, Auto-adjusted 3-D optic disk viewing from low-resolution stereo fundus image, Int. J. Comput. Biol. Med. 6 (9) (2006) 921–940.

About the Author—JUAN XU received her Bachelor degree in Electronics Department from Peking University, Beijing, P.R. China in 2001, and the Ph.D. degree from School of Electrical and Electronic Engineering, Nanyang Technological University, Singapore in 2006. She was a Software Engineer in the Stratech Systems, Singapore, from 2005 to 2006. Currently, she is a Research Scholar in the Department of Ophthalmology, School of Medicine, University of Pittsburgh, USA. Her research interests include Medical Image Processing, Computer Vision, Camera Calibration and Pattern Recognition.

Please cite this article as: J. Xu, et al., Optic disk feature extraction via modified deformable model technique for glaucoma analysis, Pattern Recognition (2006), doi: 10.1016/j.patcog.2006.10.015